

NANO EXPRESS

Open Access



Wavelength-Controlled Photodetector Based on Single CdSSe Nanobelt

Xinmin Li^{1,3}, QiuHong Tan^{1,2,3}, Xiaobo Feng^{1,2,3}, Qianjin Wang^{1,2,3} and Yingkai Liu^{1,2,3*}

Abstract

CdSSe nanobelts (NBs) are synthesized by thermal evaporation and then characterized by scanning electron microscopy (SEM), X-ray diffraction (XRD), transmission electron microscopy (TEM), high-resolution electron microscopy (HRTEM), X-ray photoelectron spectroscopy (XPS), photoluminescence (PL), and cathodoluminescence (CL). It is found that the CdSSe NBs have a good morphology and microstructure without defects. CL is sensitive to the defects of CdSSe NBs; thus, we can select single nanobelt with homogeneous CL emission to prepare a detector. Based on it, the photodetector of single CdSSe NB was developed and its photoelectric properties were investigated in detail. It is found that under illumination of white light and at the bias voltage of 1 V, the photocurrent of a single CdSSe nanobelt device is 1.60×10^{-7} A, the dark current is 1.96×10^{-10} A, and the ratio of light current to dark one is 816. In addition, the CdSSe nanobelt detector has high photoelectric performance with spectral responsivity of 10.4 AW^{-1} and external quantum efficiency (EQE) of 19.1%. Its rise/decay time is about 1.62/4.70 ms. This work offers a novel strategy for design wavelength-controlled photodetectors by adjusting their compositions.

Keywords: CdSSe nanobelts, Optical properties, Cathodoluminescence, Photodetector

Background

Recently, semiconductor nanomaterials have been widely studied as optoelectronic devices, such as light emitting diodes [1, 2], photovoltaic devices [3], solar cell [4, 5], electrocatalytic H_2 generation [6, 7], and photodetectors [8–10]. CdS and CdSe are II–VI semiconductor materials with the bandgap at room temperature of 2.42 and 1.74 eV, respectively. They are considered to be the best materials for the fabrication of photodetectors due to their bandgap corresponding to the absorption wavelength in the visible light region [11, 12].

One-dimensional nanostructures such as nanowires [13], nanobelts [14], and nanotubes [15] have been used in sensors and photodetectors due to their high surface-to-volume ratios, physical properties, and chemical properties [16]. Among them, some nanostructures such as ZnO [17], CdS [18], CdSe [19], MoS_2 [20], $\text{Zn}_x\text{Cd}_{1-x}\text{Se}$ [21], $\text{CdS}_{1-x}\text{Se}_x$ [22], and $\text{Zn}_x\text{Cd}_{1-x}\text{S}$ [23] have been used

in fabrication photodetectors. Pan et al. reported that the photodetector based on $\text{CdS}_{0.49}\text{Se}_{0.51}/\text{CdS}_{0.91}\text{Se}_{0.09}$ heterostructure has a good performance [24]. However, how to develop a high response and selectivity detector with excellent performance is still a challenge.

In this work, the CdSSe nanobelts (NBs) were synthesized by thermal evaporation. We undertake the fabrication and characterization of single CdSSe device. After that, the photoelectric properties of single CdSSe NB device were systematically investigated. Based on it, we carried out the cathodoluminescence (CL) of CdSSe NB at room temperature and low temperature and found that CL is sensitive to the defects of CdSSe NBs. Therefore, we choose nanobelts with perfect microstructures to design devices by CL so that they can achieve our desired properties.

Methods

Preparation of CdSSe Nanobelts

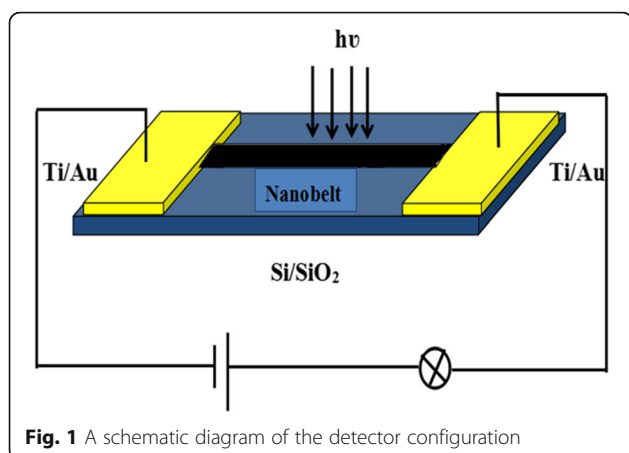
Single-crystal CdSSe NBs were prepared by thermal evaporation. For synthesis of CdSSe NBs, the mixture of pure CdS powders (99.99 wt%) and CdSe powders (9.99 wt%) pre-mixed in the weight ratio of 1:1 was put into a ceramic boat. The ceramic boat was placed in the middle of the

* Correspondence: liuyingkai99@163.com

¹Institute of Physics and Electronic Information, Yunnan Normal University, Kunming 650500, People's Republic of China

²Yunnan Key Laboratory of Opto-electronic Information Technology, Kunming 650500, People's Republic of China

Full list of author information is available at the end of the article



quartz tube. A silicon substrate coated with about 10-nm Au film was placed into the tube; the distance of silicon substrate and ceramic boat was about 5–7 cm. The furnace was heated to 820 °C and was then maintained for 2 h. Finally, the furnace naturally cooled to room temperature. The nanobelts with different compositions were deposited on the different position of the Si substrate. In the whole experiment, Ar gas was flown at 20 sccm, and the pressure inside the tube was kept at 112 Torr.

Material Characterization

The morphology, structure, and composition of the nanobelts were characterized by scanning electron microscopy (SEM), X-ray diffraction (XRD), transmission electron

microscopy (TEM), high-resolution electron microscopy (HRTEM), and X-ray photoelectron spectroscopy (XPS). The PL spectra were measured under 532-nm laser excitation. CL spectra of CdSSe NBs were measured at room temperature and low temperature by a cathodoluminescence (CL) (Gatan monocl CL4) system installed on the scanning electron microscopy (Quanta FEG 250).

Fabrication of Nanobelt Device

Ti/Au electrodes were deposited on the two ends of a single nanobelt dispersed on Si substrate with a 500-nm-thick SiO₂ layer, and then, the device was attained. The detailed fabrication process of the devices is referred in the literature [25]. The uncovered part of the nanobelts was exposed to the incident light. Figure 1 is the schematic diagram of the device test.

Photoelectric Characterization

The measurement on the photoelectric performance of nanobelts was carried out by Keithley 4200 semiconductor system and the monochromatic spectrometer. The photocurrent of the device was measured by changing the incident light vertically irradiated on the device, and I – V curves were performed by a two-probe measurement.

Results and Discussion

Figure 2a shows a SEM image of the as-prepared CdSSe NBs. It is found that the CdSSe NBs have good morphology and uniform width and lengths up to hundreds of micrometers. Figure 2b is a high magnification SEM

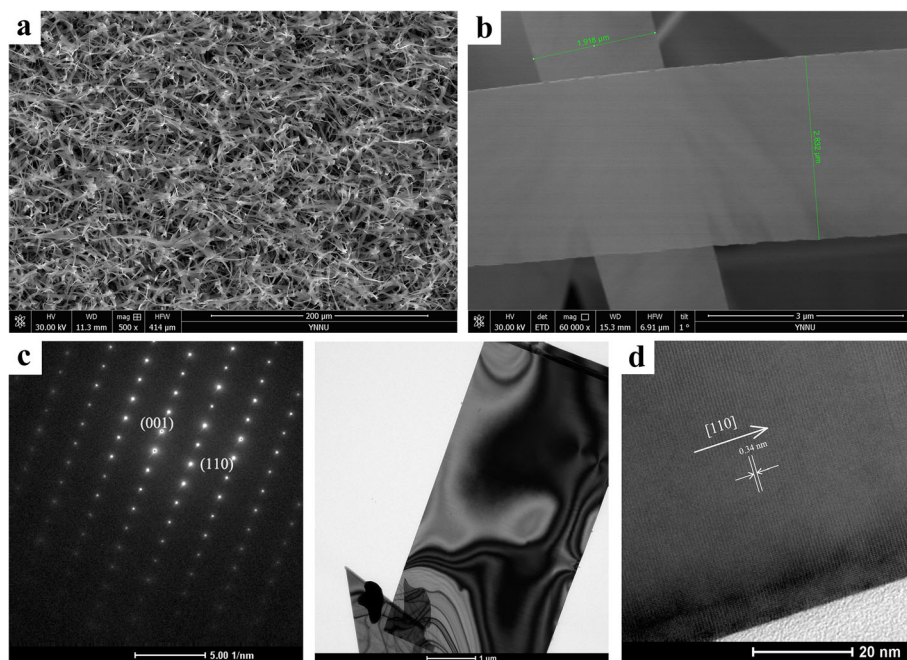


Fig. 2 The morphology images of CdSSe NBs. **a** SEM at low magnification. **b** SEM at high magnification. **c** SAD, inset: its TEM. **d** HRTEM

image of the CdSSe nanobelts. It is observed that the nanobelt is thin and uniform with 2.632 μm in width. Figure 2c and its inset present the TEM bright-field image and selected-area diffraction (SAD) pattern of a single nanobelt with a width of 2.94 μm and thickness of less than 50 nm. The SAD pattern confirms the single-crystal quality, and it can be indexed to a hexagonal structure with lattice parameters $a = 4.177$ Å and $c = 6.776$ Å. The corresponding HRTEM image is displayed in Fig. 2d, and the lattice spacing between adjacent plane is 0.34 nm, corresponding to the (110) crystal plane. Accordingly, its growth direction is along [110].

EDX and mapping of the CdSSe nanobelts are shown in Fig. 3. SEM image of a sample at low multiples is displayed in Fig. 3a. It is observed that the entire region is covered with nanobelts. Figure 3b is the total distributions of Cd, S, and Se. The mappings of Cd, S, and Se elements are depicted in Fig. 3c–e, respectively. It revealed that Cd, S, and Se are uniformly distributed in the whole nanobelts. EDX spectrum collected from the same nanobelts is presented in Fig. 3f, indicating that the nanobelt is composed of Cd, S, and Se elements.

XRD and XPS pattern of CdSSe NBs are presented in Fig. 4. All diffraction peaks can be indexed to a hexagonal structure of $\text{CdS}_{0.76}\text{Se}_{0.24}$ with lattice parameters $a = 4.177$ Å and $c = 6.776$ Å, which is consistent with the standard card (JCPDS no. 49-1459). The positions of the diffraction peaks ($2\theta = 24.72^\circ$, 26.35° , 28.13° , 36.42° , 43.47° , 47.5° , 50.4° , 51.4° , and 52.4°) matched with the crystal plane (100), (002), (101), (102), (110), (103), (200), (112), and (201), respectively. No other impurities are detected. The sharp and narrow diffraction peaks revealed that the obtained CdSSe nanobelts have good crystallinity. Figure 4b shows the binding energies of $\text{Cd}3d_{5/2}$ and $\text{Cd}3d_{3/2}$ for the CdSSe NBs at 404.8 and 411.7 eV, respectively, which are close to the values reported in the previous work [26]. The separation distance between two peaks is 6.9 eV, indicating that Cd atoms are in the complete CdS phase [27]. The deconvolution of the S(2p) peak shows two Gaussian peaks, centered at 160.7 and 165.1 eV in Fig. 4c. The valence electron spectra of Se(3d) is depicted in Fig. 4d, in which only one peak located at 53.5 eV was observed. Therefore, the XPS results confirm that the nanobelts are composed of Cd, S, and Se elements.

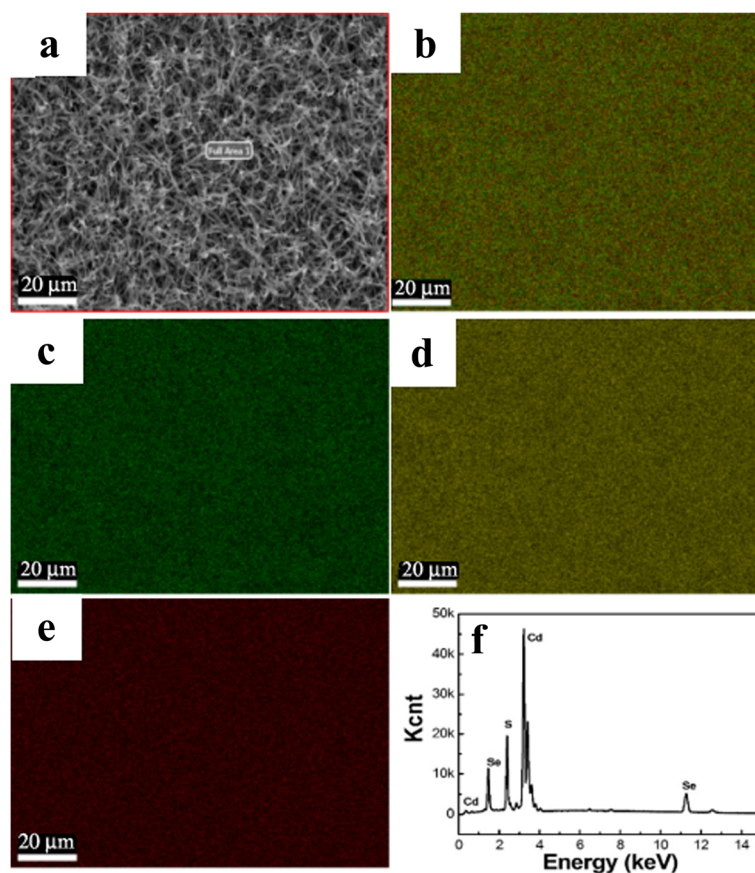


Fig. 3 SEM image and elemental mappings of CdSSe NBs. **a** SEM. **b–e** Cd, S, and Se mappings, respectively. **f** EDX

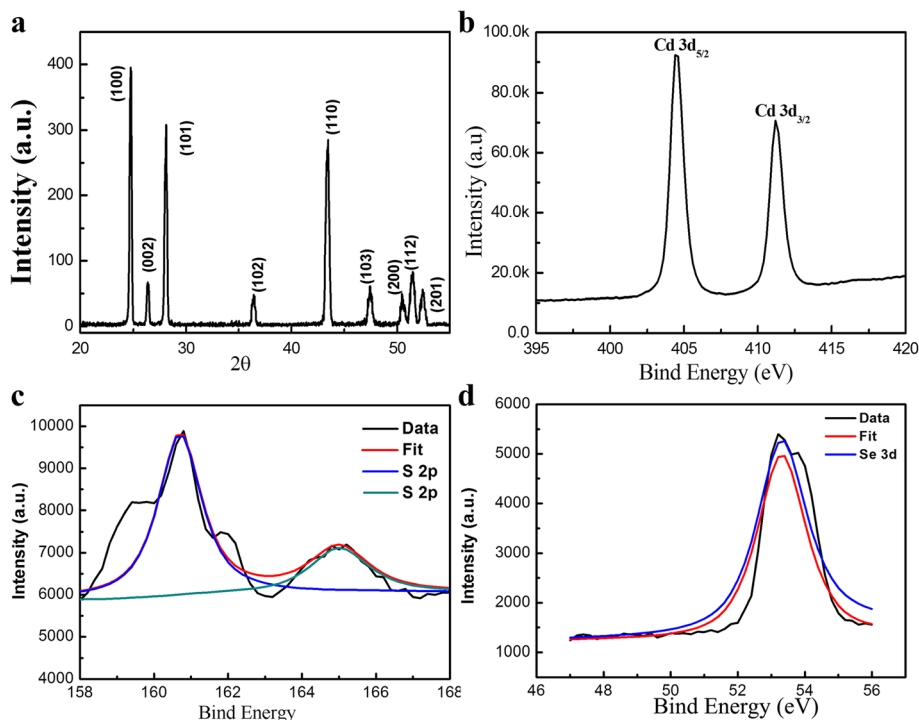


Fig. 4 XRD patterns and XPS spectra of the CdSSe NBs. **a** XRD. **b** XPS spectrum of superposed Cd(3d). **c** High-resolution XPS spectrum for S(2p). **d** High-resolution XPS spectrum for Se(3d)

Figure 5 is the photoluminescence spectrum of CdSSe nanobelts; there are two peaks in the range of 500–1000 nm. One is centered at 603 nm originated from the near-band-edge (NBE) emission of the CdSSe nanobelts. The other centered at ~ 950 nm may be related to deep-level emission, which is observed in In_2Se_3 and Ga_2Se_3 [28, 29].

SEM and CL images of the single CdSSe nanobelt are described in Fig. 6a, b. It elucidated that the surface of the nanobelts is flat and smooth and the brightness is heterogeneous along its length. Figure 6c, d is the spatial

resolution CL spectra of the same nanobelt at room temperature (295 K) and low temperature (93 K). It highlighted that the CL intensities of the characteristic NBE on CdSSe NB are different from point to point, and their signal noise ratio is not good at 295 K, whereas the CLs are strong with different intensities from point to point at 93 K. This result is in good agreement with the CL image. In addition, the characteristic peak is located at 625 nm, no defect emission is observed, and the intensity at 93 K is about 220-fold stronger than that at 295 K. Therefore, the CdSSe NB has good luminescent properties at low temperature.

Figure 7a is the SEM image of the nanodevice, which visualized that the CdSSe NB is not uniform in width. The widths of the measured NB are 30.85 and 36 μm and the length is 9.754 μm , as marked in Fig. 7a. The I – V characteristics of the CdSSe NB device is exhibited in Fig. 7b under dark conditions and white light illumination with power density of 43.14 mW/cm^2 . As can be seen, the photocurrent increases greatly under the white light irradiation, because the incident light produces electron-hole pairs, thus improving the photocurrent. The linear shape of I – V curve indicated that good ohmic contacts between the CdSSe NB and Ti/Au electrodes were formed. The photocurrent is 1.6×10^{-7} A, and the dark current is about 1.96×10^{-10} A. Therefore, the ratio of photocurrent to dark current is 816. Figure 7c is the

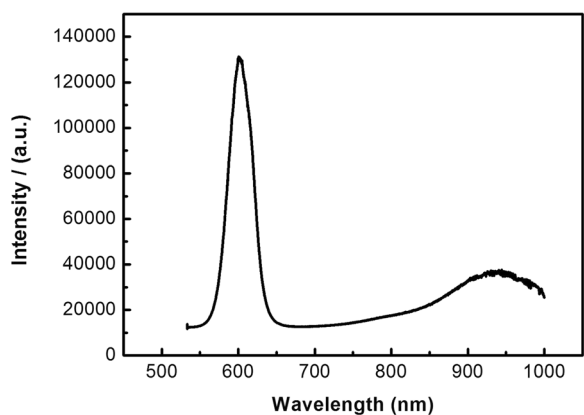


Fig. 5 The PL emission spectra of CdSSe NBs

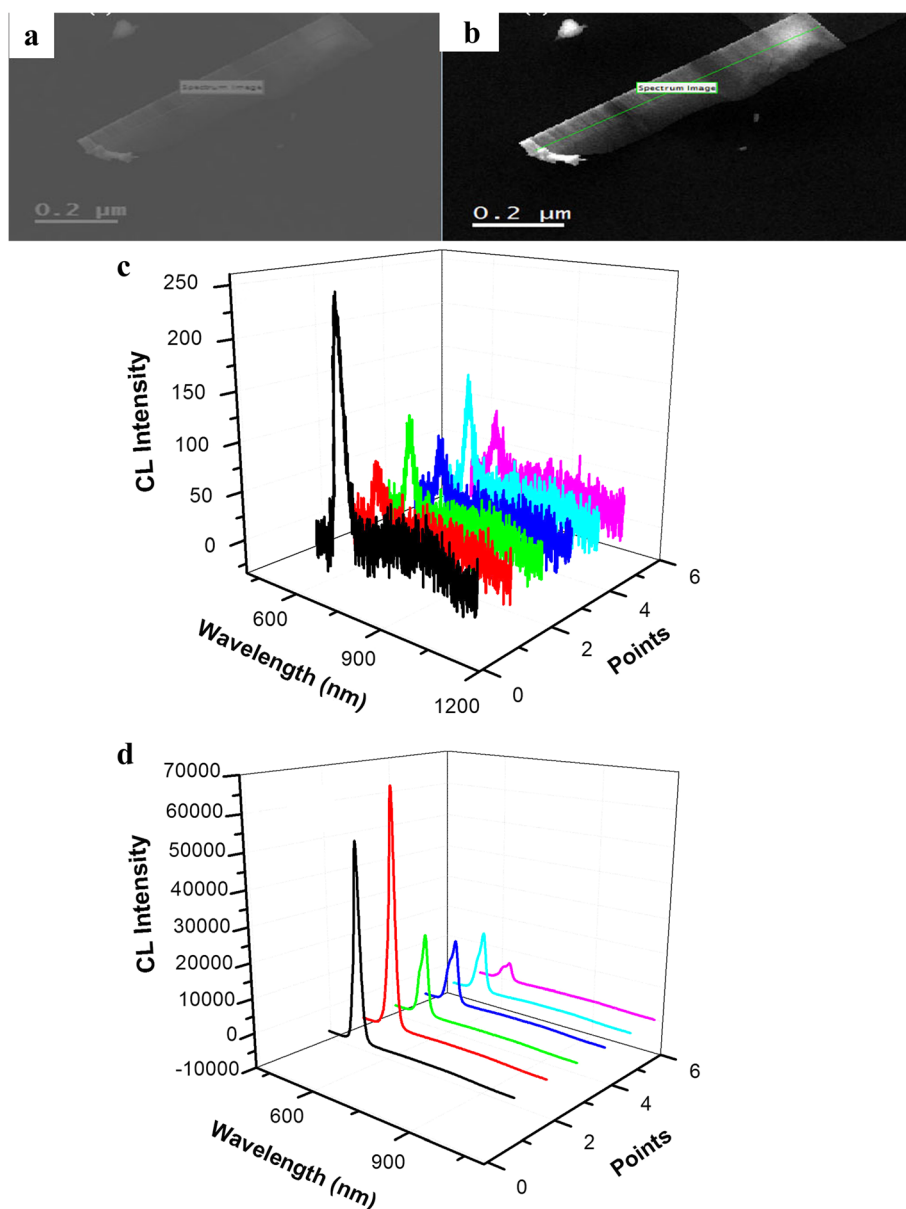


Fig. 6 SEM and CL images of a single CdSe NB. **a** SEM. **b** CL. **c** CL at 295 K. **d** CL at 93 K

I – V curve obtained after taking logarithm and found that the photocurrent is higher by three orders of magnitude than its dark current.

To further explore the photoelectronic properties of the devices, we measured the photocurrent of a single CdSe NB device, as shown in Fig. 8. At an applied biasing voltage of 1 V, the spectral response of the device in the range of 600 to 800 nm is displayed in Fig. 8a. It is seen that the response is very strong as the wavelength is less than 674 nm, and then becomes weaker and weaker when the wavelength is more than 674 nm. Figure 8b presents the measured I – V curve under illumination of 674 nm light with different power densities. It is

found that the photocurrent increases with increasing power density, implying that the photogenerated carrier efficiency is proportional to the number of absorbed photons [30]. The logarithmic plot corresponding to Fig. 8b is highlighted in Fig. 8c. It revealed that the CdSe NB device has the best response at a power density of 6.11 mW/cm^2 . Figure 8d is the relationship between the photocurrent and the optical power density. By fitting the power density-dependent photocurrent value of $I_p = AP^\theta$, where I_p is the photocurrent, P is the optical power density, A is the wavelength-dependent constant, the exponent θ determines the photocurrent response with power [31], a good fit of the experimental

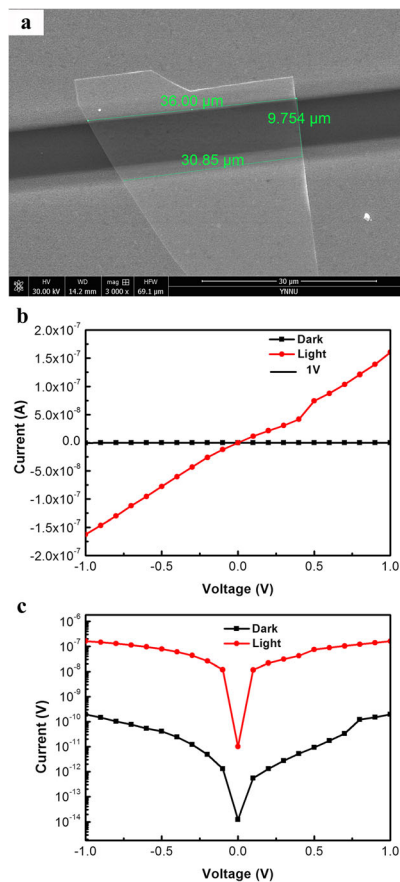


Fig. 7 SEM image and I - V curves of a single CdSSe NB detector. **a** SEM. **b** I - V curves under dark conditions and white light illumination with power density of 43.14 mW/cm². **c** I - V graph obtained after taking logarithm

results has been obtained with $\theta = 0.69$. Reports on a non-unity exponent with $0.5 < \theta < 1$ suggest a complex process of electron-hole generation, recombination, and trapping within the photoactive material [32], whereas the intensity dependence with $\theta < 0.5$ may arise owing to defect mechanisms, including both recombination centers and traps. Therefore, $\theta = 0.69$ means that CdSSe nanobelt has no defects, which is in agreement with that by HRTEM and CL.

It is well known that the spectral responsivity (R_λ) and external quantum efficiency (EQE) are critical parameters for optical devices, which can be defined as $R_\lambda = I_{ph}/(P_\lambda S)$ and $EQE = hcR_\lambda/(q\lambda)$, where I_{ph} is the difference between the photocurrent and dark current, P_λ is the light power density irradiated on the nanobelt, S is the effective illuminated area, c is the velocity of light, h is the Planck's constant, q is the electronic charge, and λ is the exciting wavelength [33, 34]. We calculated the corresponding R_λ and EQE values of the CdSSe NB device are 10.4 A/W and 19.1%.

Figure 9a shows the time response of the CdSSe NB detector, which is measured by periodically turning on and off the 674-nm light with an intensity of 4.87 mW/cm² at a bias voltage of 1 V. From that, we can see that CdSSe NB device exhibits a good reversible stability on switching properties. Figure 9b is the voltage rise and decay edge of a resistant measured by the oscilloscope. It reflects the photoconductance rise time and decay time of CdSSe NB. With and without illumination of 674-nm light (4.87 mW/cm²), the voltage of the resistant changes varies. It is seen that the rise/decay time is 1.62/4.70 ms, respectively. We compared important

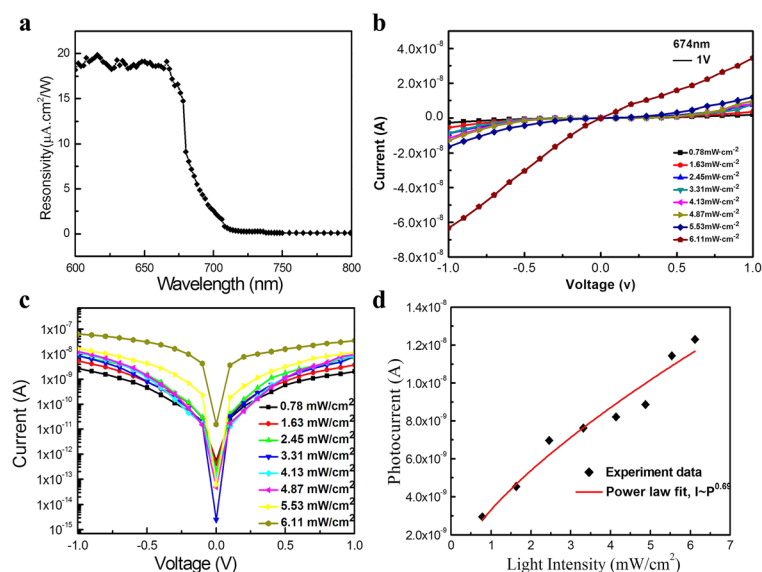


Fig. 8 The detector's photoresponse properties of the CdSSe NB detector. **a** Spectral photoresponse measured at a bias of 1 V. **b** I - V curve at the excitation wavelength of 674 nm, a bias voltage of 1 V, and different power densities. **c** The logarithmic plot of **b**. **d** The relationship between the photocurrent and the optical power density

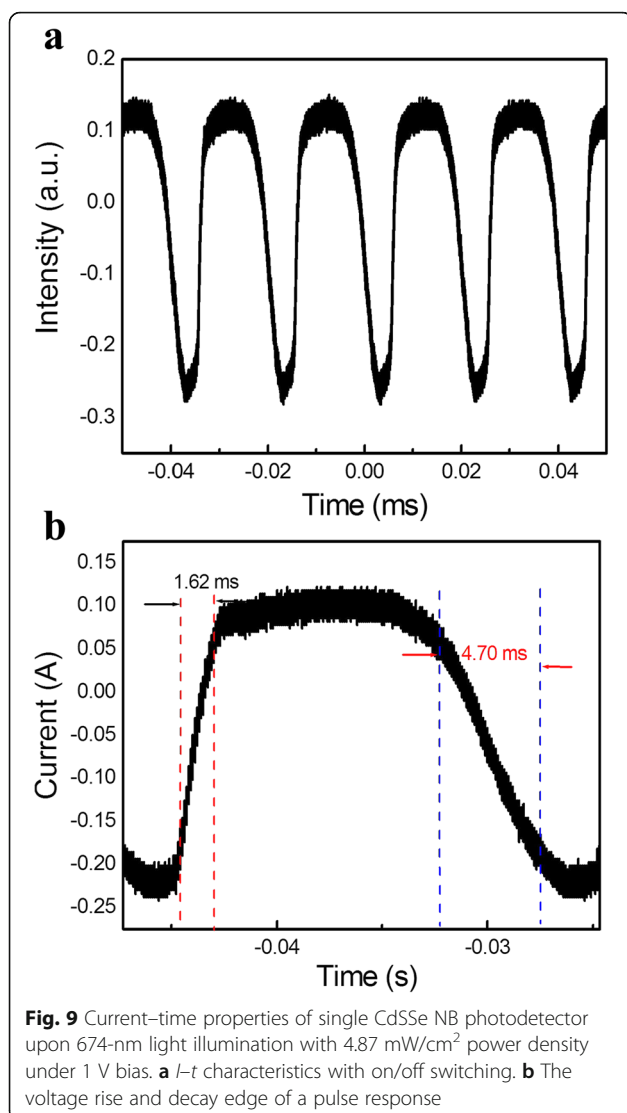


Table 1 Comparisons of important parameters of photodetectors based on single different nanobelt/nanosheet

Materials	Contact type	Response range	Responsivity	Decay time	Ref
CdS NB	OC	< 500 nm	6	20 μ s	[34]
ZnS NB	SC	UV	~ 2	< 0.3 s	[35]
BiO ₂ Se NS	OC	808 nm	6.5	2.8 ms	[36]
GaSe NS	SC	800 nm	3.5	0.1 s	[37]
SnS ₂ NS	OC	Visible	8.8×10^{-3}	5 μ s	[38]
Bi ₂ S ₃ NS	OC	Visible-NIR	4.4	10 μ s	[39]
CdSSe NB	OC	674 nm	10.4	4.7 ms	This work

Abbreviations: NB nanobelt, NS nanosheet, OC ohmic contact, SC Schottky contact

parameters of our photodetector with those of others based on single nanobelt or nanosheet (NS). It is found that the R_{λ} of the CdSSe NB device in this work is larger than that of other nanostructure photodetectors such as CdS [34] and ZnS NB [35], BiO₂Se [36], GaSe [37], SnS [38], and Bi₂S₃ NS [39]. The decay time is shorter than that of ZnS NB [35] and GaSe NS [37], but longer than that of others [34, 36, 38, 39], as summarized in Table 1, thus confirming the potential application of the CdSSe NB for photodetective field.

Conclusions

In summary, CdSSe NBs were grown in a high-temperature furnace by thermal evaporation. The obtained nanobelts were characterized by various methods. It is found that the CdSSe NBs have perfect microstructure without any defects and the nanobelts are composed of Cd, Se, and S elements. The CL results revealed that the intensity of single CdSSe nanobelt at low temperature (93 K) is stronger than that at room temperature (295 K), and the signal noise ratio is better at 93 K. After that, we developed the CdSSe photodetector based on single NB and studied its optoelectronic properties. The detector achieved high performance with responsivity of 10.4 A/W, rise/decay time of 1.62/4.70 ms, and the external quantum efficiency (EQE) of 19.1% at 674 nm, which has good stability and repeatability in the photoelectronic properties. This work paves the way towards for developing continuous-wavelength visible photodetector by tuning its composition.

Abbreviations

CL: Cathodoluminescence; EDX: Energy-dispersive X-ray; EQE: External quantum efficiency; HRTEM: High-resolution electron microscopy; NB: Nanobelt; NBE: Near-band-edge; NS: Nanosheet; PL: Photoluminescence; R_{λ} : Responsivity; SAD: Selected-area diffraction; SEM: Scanning electron microscopy (SEM); TEM: Transmission electron microscopy; XPS: X-ray photoelectron spectroscopy; XRD: X-ray diffraction

Funding

This work was supported by the National Natural Science Foundation of China (Grant No. 11764046, 11304275, and 61564010), Applied Basic Research Foundation of Yunnan Province (2017FB009), and Innovative Talents of Science and Technology Plan Projects of Yunnan Province (2014HB010).

Availability of Data and Materials

All data are fully available without restriction.

Authors' Contributions

YL guided the experiments and test process and revised the paper. LX carried out the synthesis of nanobelts and photoconductance measurement and prepared the manuscript. XF and QT carried out the characterization. QW analyzed the data. All authors read and approved the final manuscript.

Ethics Approval and Consent to Participate

Not applicable

Competing Interests

The authors declare that they have no competing interests.

Publisher's Note

Springer Nature remains neutral with regard to jurisdictional claims in published maps and institutional affiliations.

Author details

¹Institute of Physics and Electronic Information, Yunnan Normal University, Kunming 650500, People's Republic of China. ²Yunnan Key Laboratory of Opto-electronic Information Technology, Kunming 650500, People's Republic of China. ³Key Laboratory of Yunnan Higher Education Institutes for Optoelectric Information Technology, Kunming 650500, People's Republic of China.

Received: 26 April 2018 Accepted: 30 May 2018

Published online: 07 June 2018

References

- Steckel JS, Coe-Sullivan S, Bulovic Bawendi MG (2003) 1.3 μm to 1.55 μm tunable electroluminescence from PbSe quantum dots embedded within an organic device. *Adv. Mater.* 15(21):1862–1866
- Zhao J, Baardecker JA, Munro AM, Liu MS (2008) Efficient CdSe/CdS quantum dot light-emitting diodes using a thermally polymerized hole transport layer. *Nano Lett.* 6(3):463
- Li FZ, Luo LB, Yang QD, Wu D, Xie C, Nie B, Jie JS, Wu CY, Wang L, Yu SH (2013) Ultrahigh mobility of p-type CdS nanowires: surface charge transfer doping and photovoltaic devices. *Adv. Energy Mater.* 3:579
- Khosroabadi S, Keshmiri SH (2014) Design of a high efficiency ultrathin CdS/CdTe solar cell using back surface field and backside distributed Bragg reflector. *Opt. Express* 22:921–929
- Yu P, Wu J, Liu S, Xiong J, Jagadish J, Wang ZM (2016) Design and fabrication of silicon nanowires towards efficient solar cells. *Nano Today* 11:704–737
- Tong X, Zhou Y, Jin L, Basu K, Adhikari R, Selopal GS, Tong X, Zhao H, Sun S, Vomiero A, Wang ZM, Rosei F (2017) Heavy metal-free, near-infrared colloidal quantum dots for efficient photoelectrochemical hydrogen generation. *Nano Energy* 31:441–449
- Zhao Z, Qin F, Kasiraju S, Xie L, Alam MK, Chen S, Wang D, Ren Z, Wang Z, Grabow LC, Bao J (2017) Vertically aligned $\text{MoS}_2/\text{Mo}_2\text{C}$ hybrid nanosheets grown on carbon paper for efficient electrocatalytic hydrogen evolution. *ACS Catalysis* 7:7312–7318
- Rath AK, Bernechea M, Martinez L, Konstantatos G (2011) Solution-processed heterojunction solar cells based on p-type PbS quantum dots and n-type Bi_2S_3 nanocrystals. *Adv. Mater.* 23:3712
- Shafa M, Ji H, Gao L, Yu P, Ding Q, Zhou Z, Li H, Niu XB, Wu J, Wang ZM (2016) Mid-infrared photodetectors based on InSb micro/nanostructures grown on low-cost mica substrates. *Materials Lett.* 169:77–81
- Liu YK, Zhou XP, Hou DD, Wu H (2006) The photoconductance of a single CdS nanoribbon. *J. Mater. Sci.* 41:6492–6496
- Nie B, Hu JG, Luo LB, Xie C, Zeng LH, Lv P, Li FZ et al (2013) Monolayer graphene film on ZnO nanorod array for high-performance Schottky junction ultraviolet photodetectors. *Small* 9:2872–2879
- Kung SC, Ver der Veer WE, Yang F, Donavan KC (2010) 20 μs photocurrent response from lithographically patterned nanocrystalline cadmium selenide nanowires. *Nano Lett.* 10:1481–1485
- Xu S, Qin Y, Xu C, Wei YG, Yang RS, Wang ZL (2010) Self-powered nanowire devices. *Nat. Nanotech.* 5:366–373
- Fang XS, Bando Y, Liao MY, Gautam UK (2009) Single-crystalline ZnS nanobelts as ultraviolet-light sensors. *Adv. Mater.* 21:2034–2039
- An QW, Meng XQ (2016) Aligned arrays of CdS nanotubes for high-performance fully nanostructured photodetector with higher photosensitivity. *J. Mater. Sci.* 27:11952–11960
- Wu YM, Zhang H, Liu YK, Chen WW, Ma J (2015) Synthesis and gas sensing properties of single La-doped SnO_2 nanobelt. *Sensor* 15:14230–14240
- Yang SZ, Wang LF, Tian XZ, Xu Z, Wang ZL (2012) The piezotronic effect of zinc oxide nanowires studied by in situ TEM. *Adv. Mater.* 24(34):4676–4682
- Hou DD, Liu YK, Yu DP (2015) Multicolor photodetector of a single Er^{3+} -doped CdS nanoribbon. *Nanoscale Res. Lett.* 10:285
- Nusir AI, Aguilar J, Bever Z, Manasreh MO (2014) Uncooled photodetectors based on CdSe nanocrystals with an interdigital metallization. *Appl. Phys. Lett.* 104:051124
- Sanchez OL, Lembke D, Kayci M, Radenovic A, Kis A (2013) Ultrasensitive photodetectors based on monolayer MoS_2 . *Nat. Nanotechnol.* 8:497–501
- Liu Y, Zapfen JA, Shan YY, Geng CY, Lee CY (2005) Wavelength-controlled lasing in $\text{Zn}_x\text{Cd}_{1-x}\text{S}$ single-crystal nanoribbons. *Adv. Mater.* 17:1372
- Yoon YJ, Park KS, Heo JH, Park JG (2010) Synthesis of $\text{Zn}_x\text{Cd}_{1-x}\text{Se}$ ($0 \leq x \leq 1$) alloyed nanowires for variable-wavelength photodetectors. *J. Mater. Chem.* 20(12):2386–2390
- Wang L, Wang XE, Chen R, Wu CY, Yu YQ, Xu J, Hu JG, Luo LB et al (2014) Gallium doped n-type $\text{Zn}_x\text{Cd}_{1-x}\text{S}$ nanoribbons: synthesis and photoconductivity properties. *J. Appl. Phys.* 115:063108
- Guo PF, Hu W, Zhang QL, Zhang XJ, Zhu XL (2014) Semiconductor alloy nanoribbon lateral heterostructures for high-performance photodetectors. *Adv. Mater.* 26:2844–2849
- Chen C, Qin Z, Liu Y, Zhang Y, Li Y, Shen S, Wang ZM, Song HZ (2017) Promotion on acetone sensing of single SnO_2 nanobelt by Eu doping. *Nanoscale Res. Lett.* 12:405
- Chen S, Zhang X, Zhang Q, Tan W (2009) Triocetylphosphine as both solvent and stabilizer to synthesize CdS nanorods. *Nanoscale Res. Lett.* 4:1159–1165
- Baghchesara MA, Yousefi R, Cheraghizade M, Sheini FJ (2016) Photocurrent application of Zn-doped CdS nanostructures grown by thermal evaporation method. *Ceramics International* 42:1892–1896
- Okamoto T, Yamada A, Konagai M (1997) Growth and characterization of In_2Se_3 epitaxial films by molecular beam epitaxy. *J. Cry. Growth* 175/176: 1045–1050
- Okamoto T, Yamada A, Konagai M, Takahashi K (1994) Polarized photoluminescence in vacancy-ordered Ga_2Se_3 . *J. Cry. Growth* 138:204–207
- Chen G, Yu Y, Zheng K (2015) Fabrication of ultrathin Bi_2S_3 nanosheets for high-performance, flexible, visible-NIR photodetectors. *Small* 11(24):2848–2855
- Yang SX, Tongay S, Li Y (2014) Layer-dependent electrical and optoelectronic responses of ReSe_2 nanosheet transistors. *Nanoscale* 6(13):7226–7231
- Hussain AA, Sharma B, Barman T, Pal AR (2016) Self-powered broadband photodetector using plasmonic titanium nitride. *ACS Appl. Mater. Interf.* 8: 4258–4265
- Kung SC, Xing WD, Veer WE (2011) Tunable photoconduction sensitivity and bandwidth for lithographically patterned nanocrystalline cadmium selenide nanowires. *ACS Nano* 5(9):7627–7639
- Li L, Wu PC, Fang XS (2010) Single-crystalline CdS nanobelts for excellent field-emitters and ultrahigh quantum-efficiency photodetectors. *Adv. Mater.* 22:3161–3165
- Zhai TY, Li L, Wang X, Fang XS, Bando Y, Golberg D (2010) Recent developments in one-dimensional inorganic nanostructures for photodetectors. *Adv. Funct. Mater.* 20:4233
- Li J, Wang ZX, Wen Y, Chu JW, Yin L, Cheng RQ, Lei L, He P, Jiang C, Feng LP, He J (2018) High-performance near-infrared photodetector based on ultrathin $\text{Bi}_2\text{O}_3/\text{Se}$ nanosheets. *Adv. Funct. Mater.* 28:1706437
- Mukherjee B, Cai Y, Tan HR, Feng YP, Tok ES, Sow CH (2013) NIR schottky photodetectors based on individual single-crystalline GeSe nanosheet. *ACS Appl. Mater. Interfaces* 5:9594
- Chen G, Yu Y, Zheng K, Ding T, Wang W, Jiang Y, Yang Q (2015) Fabrication of ultrathin Bi_2S_3 nanosheets for high-performance, flexible, visible–NIR photodetectors. *Small* 11:2848
- Su G, Hadjiev VG, Loya PE, Zhang J, Lei S, Maharjan S, Dong P, Lou J, Peng H (2015) Fabrication of ultrathin Bi_2S_3 nanosheets for high-performance, flexible, visible–NIR photodetectors. *Nano Lett.* 15:506

Submit your manuscript to a SpringerOpen[®] journal and benefit from:

- Convenient online submission
- Rigorous peer review
- Open access: articles freely available online
- High visibility within the field
- Retaining the copyright to your article

Submit your next manuscript at ► springeropen.com